

# International Conference on Space Optics—ICSO 2022

Dubrovnik, Croatia

3–7 October 2022

*Edited by Kyriaki Minoglou, Nikos Karafolas, and Bruno Cugny,*



***Metrological setups for the optical characterization of highly compact, large aperture, fast, diffraction limited freeform Telescopes and the use of the Helmholtz-Lagrange Invariant as a criterion to assess optical design robustness***



# Metrological setups for the optical characterization of highly compact, large aperture, fast, diffraction limited freeform Telescopes and the use of the Helmholtz-Lagrange Invariant as a criterion to assess optical design robustness

P. Sandri<sup>\*a</sup>, A. Boni<sup>a</sup>, M. Deiml<sup>a</sup>, M. Erhard<sup>a</sup>, M. Freudling<sup>a</sup>, P. Muraro<sup>a</sup>, T. Sedlmaier<sup>a</sup>  
<sup>a</sup>OHB System AG - Manfred-Fuchs-Str. 1, D-82234 Weßling, Germany

## ABSTRACT

The paper presents the metrological setups for the optical measurements of two high quality, large aperture, extremely compact, diffraction limited, relative aperture 1:2.4 free-form telescopes: the CHI and the TIR. The CHI “Compact and Highly Performing Hyperspectral Imager“, is based on a Three-Mirror Anastigmat (TMA) layout and works in the spectral range 0.4-2.5 $\mu$ m with 150 mm aperture. The Thermal Infrared (TIR) Telescope is based on a two-powered-mirror design and works in the spectral range 10-12  $\mu$ m with 140 mm entrance aperture. Both free-form Telescopes have been designed by OHB Germany and are currently under production at SPACEOPTIX GmbH / Fraunhofer IOF and at VDL ETG / SUMIPRO, respectively. The measurement campaign consists in measuring the wavefront error all over the field of view at 633 nm, the focal length across- and along-track and the geometric distortion. The paper focuses attention on the TIR freeform Telescope. To support the optical tests preparation, the TIR free-form Telescope is analyzed with a pure geometrical optic approach, making also use of the Helmholtz-Lagrange Invariant. The definition of the Helmholtz-Lagrange Invariant for an axial field is recalled from the classic literature. Then the optical invariant of the paraxial optic is extended to the real ray-tracing of the TIR Telescope both in its nominal layout and when subjected to the manufacturing, alignment and integration (MAIT) tolerances. In this way, the optical invariant represents a method, complementary to the commonly used ones, for evaluating the quality of an optical design and for assessing its robustness to the MAIT tolerances.

**Keywords:** freeform optic, Helmholtz-Lagrange invariant, sine condition, Staebler and Lihotzky.

## 1. INTRODUCTION

In the recent years freeform optics is continuously gaining wider fields of applications for the advantages offered in compacting the design packaging and for allowing large Field of Views, see e.g. [1], [2], [3], [4] and [5]. Furthermore, the development of the fabrication techniques and of the metrology techniques, together with innovative alignment approaches, as for example the snap-in approach [6], make the freeform all-metal telescopes a very interesting solution for space optics. This paper describes first the main design characteristics of the Telescope and then the performance verification approach. In the last Section, the Helmholtz-Lagrange invariant is used to have a first assessment of the robustness of the design wrt the MAIT tolerances.

## 2. THE TIR FFO TELESCOPE

OHB Germany has recently designed two fast and large aperture freeform Telescopes: the first one is named CHI *Compact highly performant Hyperspectral Imager* and is based on a Three Mirror Anastigmatic (TMA) layout, working in the spectral range 0.4-2.5 $\mu$ m with a relative aperture F/2.4 and a front aperture of 150 mm, see [7].

The second is a Thermal Infrared (TIR) Telescope, with spectral band 10-12 $\mu$ m, based on a two-powered-mirror, extremely compact, thanks to the freeform design, diffraction-limited on the entire FoV, presenting a relative aperture F/2.4 and an entrance aperture of 140 mm. Both Telescopes are at the moment under production: the CHI at SPACEOPTIX GmbH and Fraunhofer IOF and the TIR at VDL ETG / Sumipro.

\*paolo.sandri@ohb.de; phone +49 8153 4002-547; fax +49 8153 4002-940; www.ohb.de

Being the CHI already presented in [7], we dedicate this Section to the TIR telescope. Table 1 summarizes the main properties of the Telescope, the working field of View and the volume constraint. Figure 1 shows the mechanical layout of the TIR Telescope and the ray-tracing. In right panel of Figure 1 different colors correspond to different FoVs.

Table 1 Main optical data of the TIR freeform telescope.

Entrance Pupil diameter [mm]	140
Relative aperture F/number	2.4
Spectral band [ $\mu\text{m}$ ]	10 - 12
ACT /ALT FoV [ $^\circ$ ]	$\pm 1.65^\circ / \pm 0.19^\circ$
Volume constraint $\text{mm}^3$	200 x 200 x 300
Field average RMS WFE @10 $\mu\text{m}$ – nominal design	0.056
Field average RMS WFE @10 $\mu\text{m}$ – worst case of 3000 MC runs	0.070

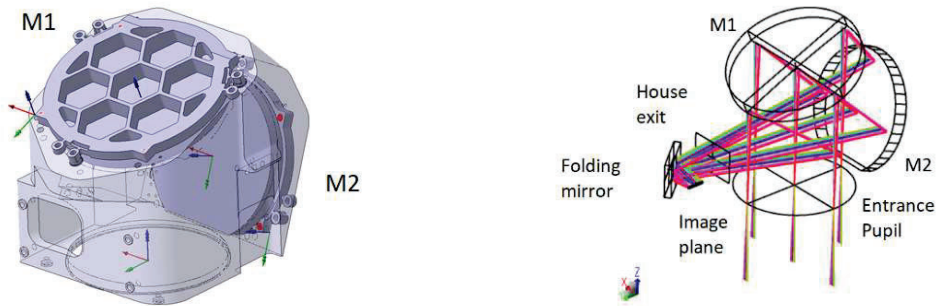


Figure 1. TIR freeform Telescope. Left / Right: opto-mechanical assembly / ray-tracing.

Both free-form mirrors M1 and M2 are tilted around the X and Y local axis. The orientation of the mirrors has been used as an optimization degree of freedom, both for image quality optimization and for compacting the volume. One edge of the mirror M2 is quite close to entrance aperture. Therefore to avoid beam vignetting, the mirror has a side cut, slightly tilted at  $1.5^\circ$  following the orientation of the footprint of the beams, as shown in right panel of Figure 2.

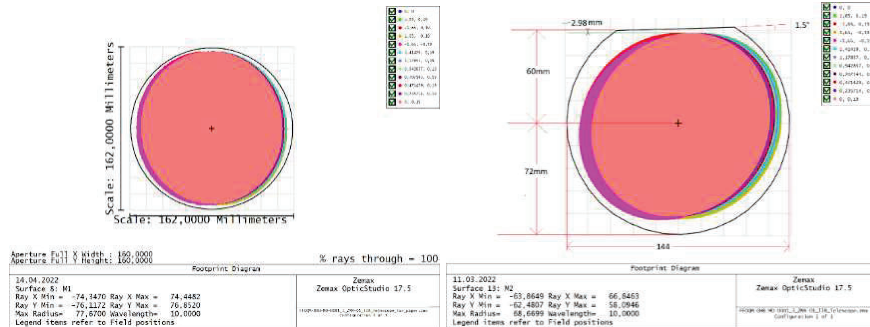


Figure 2. Left / Right: Footprint on M1 / M2 of the TIR freeform Telescope. Different colors correspond to different FoVs.

The polychromatic spot diagram, the Seidel diagram and the worst case WFE of the TIR freeform Telescope are respectively shown in left, center and right panel of Figure 3. Interesting is to note that the TIR freeform Telescope presents only residual spherical aberration, approx.  $80 \mu\text{m}$ , and a little contributor of coma, few micrometers, as reported in central panel of Figure 3.

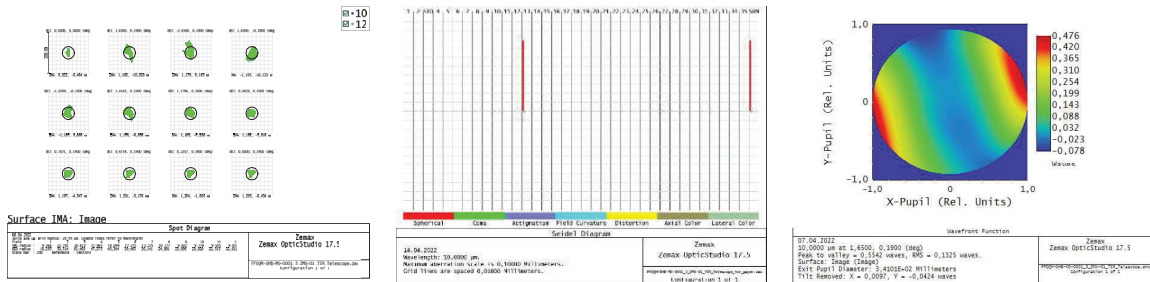


Figure 3 Left / center / right: Spot diagrams, Seidel diagrams, worst case WFE of the TIR freeform telescope.

The next Sections present the first order properties of the TIR Telescope derived with geometric optics and the set-ups for the planned optical measurements of both freeform CHI and TIR Telescopes.

### 3. FOCAL LENGTH AND DISTORTION FROM GEOMETRICAL OPTICS

The mathematical description of freeform surfaces is generally achieved by means of orthogonal polynomials, e.g. the Zernike, the 2D-Q polynomials, the Chebyshev Polynomial surface, see for details [8], [9], [10] and [11]. Both for the CHI and TIR Telescope the Zernike Polynomial surfaces have been used. As in presence of freeform surfaces optical CADs might provide in the *optical prescription data* incorrect data for the first order properties, we support the OGSE definition by calculating the first order properties of the TIR Telescope with geometric optic. From the optical Zemax model the angle  $u'$  of the axial marginal ray in the image space is extracted. Then the numerical aperture in the image space is calculated with the formula  $NA = n' \cdot \sin(u')$ , being  $n'$  the refractive index in the image space. To evaluate the focal length  $f$  different approaches can be followed. We prefer to use the special form of the *isoplanatism condition*, that is the *sine condition*, as we find this approach interesting.

It is known that in the frame of the Theory of the Seidel aberrations, the knowledge of the amount of the spherical aberration  $\sum A_v$  and of the asymmetric aberrations  $\sum B_v$  allows, by means of the Fraunhofer relation  $\frac{1}{z_1} = \frac{1}{s_1} + \frac{1}{n_1} \frac{\sum A_v}{\sum B_v}$ , to find a position  $z_1$  of the Exit Pupil that makes the system isoplanatic. In the previous formula  $s_1$  is the input conjugate and  $n_1$  the refractive index in the object space, see [12] and [13]. Nevertheless, for fast optical system the fulfilling of the Fraunhofer condition is not enough to guarantee the absence of asymmetric aberration. A criterion for the absence of asymmetric aberration and for guaranteeing an amount of spherical aberration in zonal and marginal beams equal to that of the axis, was found almost contemporary by Staebble and Lihotzky, in 1919. This is the so called *isoplanatism condition*, expressed by Staebble and Lihotzky with the formula, see [13]:

$$S'_k - s'_k = \frac{s'_k - z'_k}{\beta'_s} \left\{ \frac{n_1 \sin(u_1)}{n_k \sin(u_k)} - \beta'_s \right\} \quad (1)$$

In (1)  $S'_k - s'_k$  is the axial distance between the real image position and the paraxial one,  $\beta'_s$  is the lateral magnification,  $z'_k$  is the position of the asymmetric error free exit pupil,  $u_1$  and  $u'_k$  are the angles of the axial marginal ray wrt the optical axis in the object and in image space,  $n_1$  and  $n'_k$  the refractive index in the object and in the image space. The axial marginal ray making an angle  $u$  with the optical axis intercepts the axis in the image space at the distance  $S'_u$  from the last surface. For an object set at infinity,  $s_1 \cdot \sin(u_1) \rightarrow H_1$  and  $s_1 \cdot \beta'_s \rightarrow f_1$  the (1) assumes the special form:

$$S'_k - s'_k = \frac{s'_k - z'_k}{f} \left\{ \frac{n_1 H_1}{n_k \sin(u_k)} - f \right\} \quad (2)$$

with  $H_1$  the marginal ray intercept at first surface of the optical system and  $f$  the focal length. For a homocentric system ( $S'_u = s'$ ), with refractive index 1 in object and image space, formula (2) reduces to:

$$f = \frac{H_1}{n' \cdot \sin(u)} \quad (3).$$

The above formula (3) is used for the evaluation of the focal length of the TIR Telescope from the design data, see Table 2, regardless of the fact that the TIR Telescope is not completely homocentric, see right panel of Figure 3, considering negligible the contributor of the residual spherical aberration ( $\approx 80\mu\text{m}$ ) to the focal length value. Following Table 2 reports the marginal ray angle  $u'$  for the axial field of view for ACT and ALT in plus and minus directions, the numerical aperture

and the resulting effective focal length. In the laboratory, the focal length both in across- and along- direction is evaluated as the ratio of the centroid height  $\tilde{l}_k$  to the tangent of the subtended angle, that is:

$$f_i = \frac{\tilde{l}_k}{\tan(w_i)} \quad i = ACT, ALT \quad (4).$$

Formula (4) is valid in the paraxial regime. The assumption is that for small incident angles the centroid height and the paraxial height coincide, that is  $\tilde{l}_k \approx l_k$ .

Table 2 Main optical data of the TIR freeform telescope.

ACT direction		ALT direction	
Marginal ray (0,0,1,0) angle [°]	12,13	Marginal ray (0,0,0,1) angle [°]	11,24
Marginal ray (0,0,-1,0) angle [°]	12,14	Marginal ray (0,0,0,-1) angle [°]	11,45
NA (0,0,1,0)	0,210	NA (0,0,0,1)	0,195
NA (0,0,-1,0)	0,210	NA (0,0,0,-1)	0,199
Focal length ACT direction [mm]	333,04	Focal length ALT direction [mm]	359,16

The geometric distortion  $D_i$  of the TIR Telescope is evaluated with the classical formula:

$$D_i = \frac{l_k - \tilde{l}_k}{l_k} \quad i = ACT, ALT \quad (5).$$

#### 4. OPTICAL MEASUREMENTS DESCRIPTION: WFE, FOCAL LENGTH, DISTORTION

This Section describes the Optical Ground Space Equipment (OGSE) for the characterization of the CHI and the TIR Telescope. The optical characterization will take place in an ISO8 optical laboratory.

##### 4.1 Set-up for the WFE

The WFE measurement in double pass is performed with a Zygo 6” aperture interferometer installed on an anti-vibration optical bench. The Telescope under test, see left panel of Figure 4, and the spherical concave back cavity mirror - Melles Griot-09LRS f/075 with  $\lambda/50$  surface quality, see central panel of Figure 4 - are installed on an optical bench, placed on a hexapod in front of the Interferometer. The beam provided by the interferometer illuminates also the reference surfaces machined and polished in the nearby of the entrance aperture of the TIR Telescope – see right panel of Figure 4, allowing for a relative alignment between the Interferometer and the Telescope, for which we assigned a requirement of 20 arcsec.

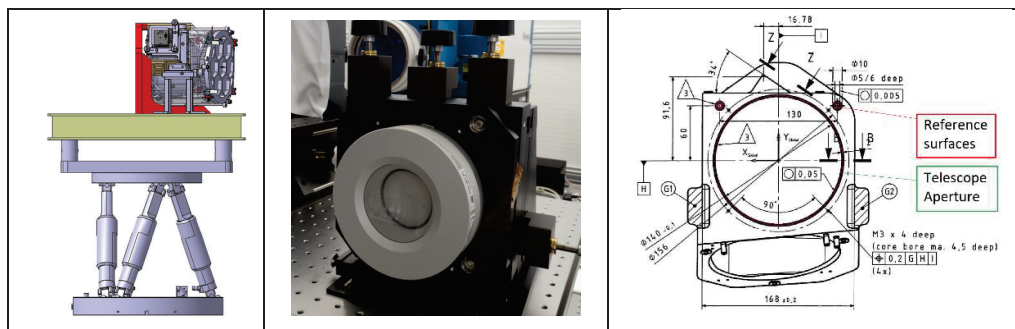


Figure 4 Left / Center / Right: TIR Telescope on the optical bench / back cavity mirror / frontal view of the Housing of the TIR Telescope with the Alignment features.

Figure 5 shows the conceptual set-up for the WFE measurement of the TIR Telescope. The collimated beam of the interferometer feeds the Telescope under test. The back cavity mirror is confocal with the Telescope. For the TIR Telescope a tilted support might be necessary. The WFE is measured on axis and for different ACT and ALT FoVs reaching the maximum values of Table 1. The Telescope can be made working at the different FoVs in ACT and ALT directions through rotations driven by the Hexapod.

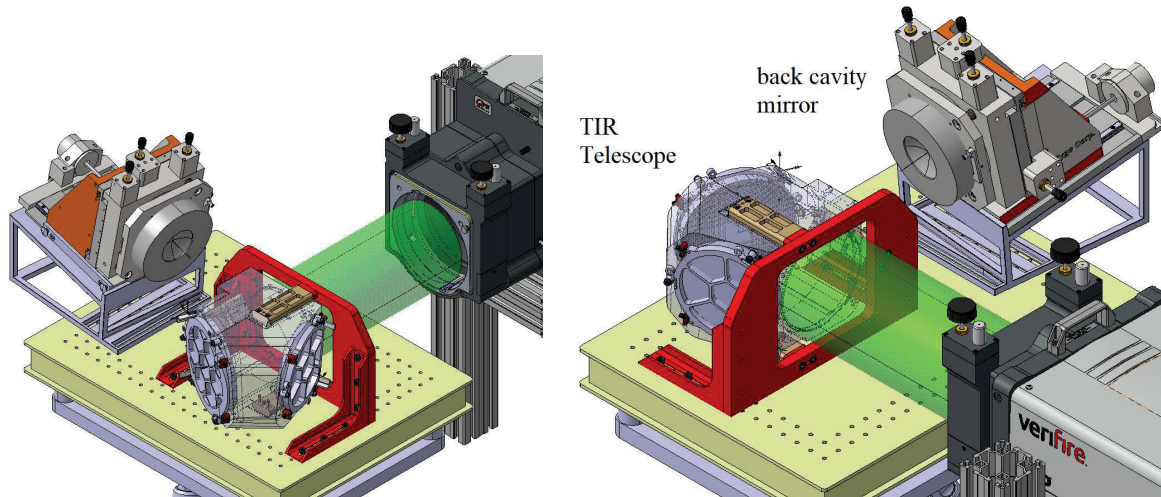


Figure 5 Conceptual set-up for the WFE measurement of the TIR freeform Telescope.

#### 4.2 Set up for the focal length and geometric distortion

The effective focal length and the geometric distortion of the TIR telescope are measured by means of a Möller-Wedel 140 mm focal length, 28 mm clear aperture autocollimator, model 5/140 and an auxiliary camera uEye IDS model UI-1450C. This autocollimator is selected among the different ones available in OHB optical Laboratory, despite of its short focal length, as it presents a set of selectable targets, which are helpful in finding the position of the image plane when installing and aligning the auxiliary camera on the image plane of the Telescope. Other autocollimators with longer focal length, e.g. 500 mm with 52 mm entrance Aperture, model Möller-Wedel 10/500, are available and might be used to reduce the uncertainty in the measurement of the focal length, taking benefit of their larger pupil diameter.

The telescope and the camera are installed on the optical bench, which in turn is mounted on the Hexapod. The camera is mounted on a 5 axes adjustable stage. The Autocollimator is mounted on a dedicated support, in front of the optical bench holding the Telescope. The position of the Autocollimator is kept fixed, whereas the position of the Telescope can be adjusted in horizontal and vertical position, and in angular orientations through the Hexapod. First, the Autocollimator position is adjusted such that its beam illuminates the Alignment features machined in the Housing of the Telescope. After a relative alignment between autocollimator and TIR Telescope, better than 20 arcsec, is achieved, the position of the Telescope is moved to have that the beam of the collimator illuminates (almost) the centre of the Telescope Aperture.

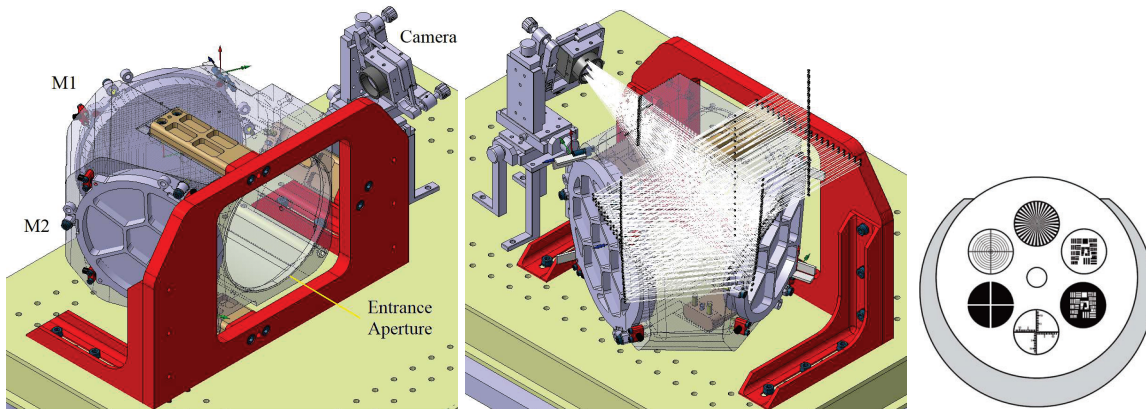


Figure 6 Left: TIR Telescope from the Entrance Aperture. Central: ray-tracing. Right: Targets in the Möller-Wedel AK 5/140.

The USAF Resolution target is selected in the Möller-Wedel Autocollimator 5/140, see right panel of Figure 6. The position and orientation of the auxiliary camera is then adjusted until its image results well sharp. With the AK 5 / 140 the depth of Focus is approximately  $\pm 85 \mu\text{m}$ . For the focal length and geometric distortion measurements is instead a cross-line target used. The set-up is shown in Figure 7 and Figure 8.

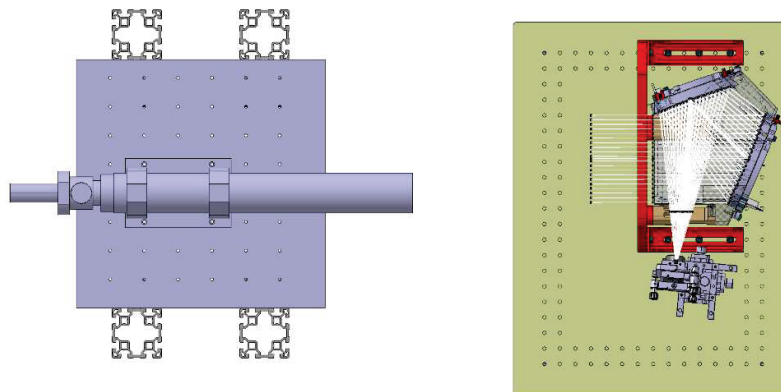


Figure 7 Top view of the Set-up for the focal length and distortion measurement.

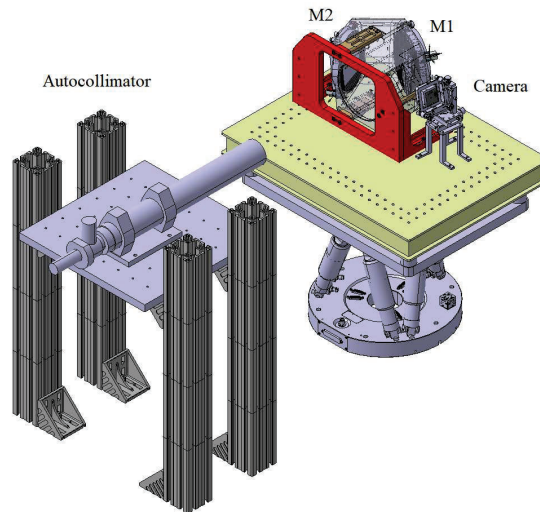


Figure 8 Set-up for the focal length and distortion measurement.

The effective focal length will be derived from the measured data by means of formula (4) and compared with the theoretical data of Table 2. The geometric distortion will be derived from the measured data with formula (5).

## 5. HELMHOLTZ-LAGRANGE INVARIANT

A deeper understanding of the TIR freeform telescope is gained by means of the Helmholtz-Lagrange invariant, e.g. [12], [13], [14]. In some References the invariant is called Smith-Helmholtz, [14], in others simply *optical invariant* [15]. In [15] the operand LINV is available to compute the paraxial optical invariant.

In the frame of the geometric optic the simplified form of the Helmholtz-Lagrange invariant for an axial field is defined, with reference to left panel of Figure 9, see [13], as:

$$n_1 \cdot l_1 \cdot u_1 = n'_k \cdot l'_k \cdot u'_k \quad (6)$$

$$n_1 \cdot q_1 \cdot w_1 = n'_k \cdot q'_k \cdot w'_k \quad (7)$$

being  $l_1$  and  $l'_k$  respectively the object and image paraxial heights,  $q_1$  and  $q'_k$  respectively the entrance pupil and the exit pupil paraxial height. Formulas (6) and (7) take benefit of the fact that for small angles  $\cos(u_1) = \cos(u'_k) = 1$ ,  $du_1 = u_1$  and  $du'_k = u'_k$ . By subtracting both members in eqs. (6) and (7) one obtains for the change in the invariant in the frame of paraxial optic, as expected:

$$\Delta I = (n_1 \cdot q_1 \cdot w_1 - n'_k \cdot q'_k \cdot w'_k) - (n_1 \cdot l_1 \cdot u_1 - n'_k \cdot l'_k \cdot u'_k) = 0 \quad (8).$$

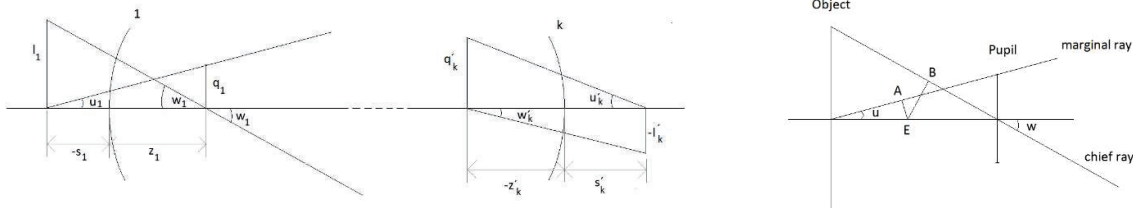


Figure 9 Ray-trace from object space to image space. Left as per [13]. Right as per [12].

It is worth seeing that (8) in other references, e.g. [12], is named  $LLW = der\ lineare\ Leitwert$ , being the quantity defined, with reference to right panel of Figure 9, as:

$$LLW = AnW - BnU \quad (9)$$

where  $A$  and  $B$  are respectively the length of the segment originating from a point  $E$  laying on the optical axis and being perpendicular to the marginal and chief ray,  $U = \sin(u)$  and  $W = \sin(w)$ . For a deeper discussion of the  $LLW$  system invariant and its application see [12] and [16]. It is also worth noting that (8) and (9) are equivalent by means of a coordinate transformation, meaning that the Helmholtz-Lagrange Invariant is independent from the chosen coordinate system.

Repeating the exercise reported in [12], with the help of left panel of Figure 10, one obtains  $LLW = \frac{\bar{A}}{\bar{U}} - \frac{\bar{B}}{\bar{W}} = \frac{A}{\cos u} \frac{\cos u}{\sin u} - \frac{B}{\cos w} \frac{\cos w}{\sin w} = \frac{A}{U} - \frac{B}{W}$  being  $\bar{A}$  and  $\bar{B}$  the length of the segment originating on the chief and on the marginal ray and perpendicular to the optical axis and  $\bar{U} = \tan(u)$  and  $\bar{W} = \tan(w)$ .

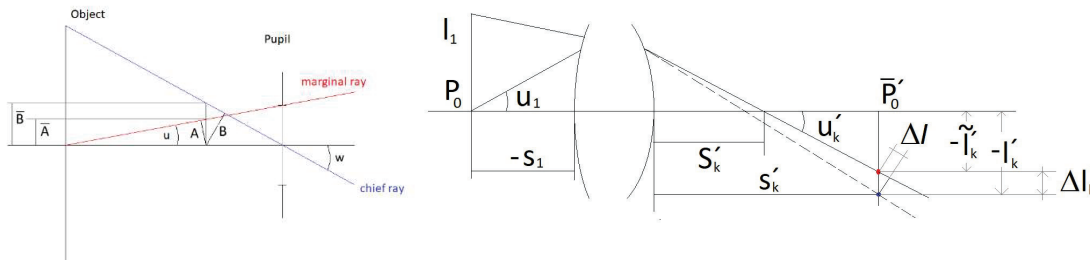


Figure 10 Left: Characteristics lengths for the optical invariant in 2 coordinate systems. Right: Ray-trace in a tangential section.

## 6. HELMHOLTZ-LAGRANGE INVARIANT OF THE TIR FREEFORM TELESCOPE

The optical quality of the designed TIR freeform Telescope, during the OGSE preparation, is assessed – as commonly done - by means of the spot diagrams, of the MTF curves and of the theoretical WFE. To deepen our understanding of the TIR Telescope we extend the optical invariant of the paraxial optic to the real ray-tracing following in part the approach of Ref. [12], where the  $LLW$  is applied to an air-spaced Triplet to check the correctness of the ray-tracing. As at the image plane  $q_k = 0$ , formula (8) can be rewritten as:

$$\Delta I = n_1 \cdot q_1 \cdot w_1 - (n_1 \cdot l_1 \cdot u_1 - n'_k \cdot l'_k \cdot u'_k) = 0 \quad (10).$$

The evaluation of the term  $n_1 \cdot q_1 \cdot w_1$  in (10) is straightforward. To evaluate the term  $(n_1 \cdot l_1 \cdot u_1 - n'_k \cdot l'_k \cdot u'_k)$  in (10) in presence of aberrations, we use the graphic representation of the right panel in Figure 10, where an Object with size  $l_1$  is imaged into the image space. The paraxial image identified by the dashed ray has the size  $l'_k$  while the real image identified by the continuous ray has the size  $\tilde{l}'_k$ . The quantity  $\Delta l'_k$  denotes the total amount of aberration. In Figure 10 its tangential component is represented.

Formula (6) in its general form can be applied to the paraxial heights  $l_1$  and  $l'_k$ , obtaining:

$$n_1 \cdot l_1 \cdot \cos(u_1) \cdot du_1 - n'_k \cdot l'_k \cdot \cos(u'_k) \cdot du'_k = 0 \quad (11)$$

and by making use of the relation  $l'_k \approx \tilde{l}'_k - \Delta l'_k$  the (11) becomes:

$$n_1 \cdot l_1 \cdot \cos(u_1) \cdot du_1 - n'_k \cdot \tilde{l}'_k \cdot \cos(u'_k) \cdot du'_k + n'_k \cdot \Delta l'_k \cdot \cos(u'_k) \cdot du'_k \approx 0 \quad (12)$$

or equivalently:

$$l_1 \cdot d(n_1 \cdot \sin(u_1))'_k - \tilde{l}'_k \cdot d(n'_k \cdot \sin(u'_k)) + \Delta l'_k \cdot d(n'_k \cdot \sin(u'_k)) \approx 0 \quad (13).$$

Formula (13) can be easily integrated, obtaining:

$$n_1 \cdot l_1 \cdot \sin(u_1) - n'_k \cdot \tilde{l}'_k \cdot \sin(u'_k) + \Delta l'_k \cdot n'_k \cdot \sin(u'_k) \approx 0 \quad (14).$$

Formula (10) in its general form, after integration, in presence of aberrations becomes:

$$\Delta I = n_1 \cdot q_1 \cdot \sin(w_1) - [n_1 \cdot l_1 \cdot \sin(u_1) - n'_k \cdot \tilde{l}'_k \cdot \sin(u'_k) + \Delta l'_k \cdot n'_k \cdot \sin(u'_k)] \approx 0 \quad (15).$$

Being  $n_1 u_1 = 0$  for a Telescope set at infinity, one obtains that the change in the invariant from object to image space in presence of aberrations is approximately equal to the total amount of aberration times the image space numerical aperture, that is:

$$\Delta I = n_1 \cdot q_1 \cdot \sin(w_1) + n'_k \cdot \tilde{l}'_k \cdot \sin(u'_k) \approx \Delta l'_k \cdot n'_k \cdot \sin(u'_k) \quad (16)$$

or equivalently:

$$\Delta l'_k \approx 2 \cdot \Delta I \cdot b \quad (17).$$

being  $b$  the image space relative aperture derived from the numerical aperture with the formula:  $n'_k \cdot \sin(u'_k) = \frac{1}{2b}$ . Right panel of Figure 10 shows a graphical interpretation of the relation between the change in the Invariant and the tangential aberration, in the frame of the Seidel Theory.

Formula (16) results to be useful for evaluating the total amount of residual aberration, especially for freeform telescopes when, due to large departure from classical surfaces, the optical CAD might not succeed in evaluating the Seidel aberrations and the first order parameter. An example of such a telescope is the freeform CHI, shortly discussed in the next Section.

The real image height in (16) is evaluated with the relation  $\tilde{l}'_k = \sqrt{X_{(1,1,0,0)}^2 + Y_{(1,1,0,0)}^2} - \sqrt{X_{(0,0,0,0)}^2 + Y_{(0,0,0,0)}^2}$ , where  $X_{(1,1,0,0)}$  and  $Y_{(1,1,0,0)}$  denote respectively the X- and Y-centroid positions for the normalized field height and pupil coordinates ( $H_x=1, H_y=1, P_x=0, P_y=0$ ), according to the Zemax notation [15]. The above formula for  $\tilde{l}'_k$ , taking into account also for possible shift of the axial image point due to MAIT tolerances, is useful in the next Section where the effect of the MAIT tolerances is considered. With the data of Table 1 the radial marginal height for the TIR Telescope results  $\tilde{l}'_k = 9.6118mm$ . Following Table 3 reports the result for the Helmholtz-Lagrange invariant  $I$  for the nominal design of the TIR Telescope.

Table 3 Helmholtz-Lagrange Invariant of the nominal design of the TIR freeform Telescope.

At the entrance Aperture		At the image plane	
Semi-Entrance Pupil [mm]	70,00	Radial Marginal ray angle [°]	-9,6118
Radial FoV (1.65°, 0.19°) [°]	1,6609	NA (0,0,1,0)	0,2102
$n_1 \cdot q_1 \cdot \sin(w_1)$ [mm]	2,0289	$n'_k \cdot \tilde{l}'_k \cdot \sin(u'_k)$ [mm]	-2,0203

The change in  $I$  for the nominal design of the TIR freeform Telescope from object to image space results less than 1 wave @  $10\mu\text{m}$ , which is in line with the dimension of the spot diagram and with the worst case WFE PV, respectively reported in the left and in the right panels of Figure 3. By applying (17) to the TIR Telescope one finds for the total amount of aberrations:  $\Delta l'_k \approx 2 \cdot b \cdot \Delta I = 2 \cdot 2.37 \cdot 8.6\mu\text{m} \approx 40.9\mu\text{m}$ . The optical CAD reports approximately  $78\mu\text{m}$  of spherical aberration and  $-2\mu\text{m}$  of coma in central panel of Figure 3. A quite good agreement when considering that the analysis is limited to the Seidel Aberrations.

### 7. HELMHOLTZ-LAGRANGE INVARIANT OF THE TIR WITH MAIT TOLERANCES

The TIR Telescope was subjected during the designing phase to a tolerance analysis, consisting in statistically combining the MAIT tolerances. We are now interested in the statistic of the term  $\Delta l'_k \cdot n'_k \cdot \sin(u'_k)$  and of the commonly used image quality parameters, as the WFE rms and the Spot rms. The results for the entire population of 3000 Montecarlo runs are shown in following Table 4 together with the values of the nominal design.

Table 4 Helmholtz-Lagrange Invariant, WFE rms, spot rms of the TIR freeform Telescope including MAIT tolerances.

	$ I $ at image plane [mm]	WFE_RMS axis [nm]	WFE_RMS Max FoV [nm]	RMS_SPOT axis [mm]	RMS_SPOT FoV_max [mm]
Nominal	2,020	490,567	1323,452	0,010	0,023
Max.	2,024	781,375	1578,086	0,015	0,028
Min.	2,003	346,989	1078,572	0,007	0,019
Average	2,021	521,186	1333,196	0,011	0,023
St. dev.	0,002	63,683	81,156	0,001	0,001

The standard deviation of the  $I$  in the Image plane is approximately equal to the Rayleigh  $\lambda/4$  criterion, allowing to conclude for a robust optical design to the selected set of MAIT tolerances.

### 8. CHI FREEFORM TELESCOPE AND A PETZVAL LENS

The above approach is now applied to the CHI Telescope [7] and to a pure refractive design, as a Petzval Portrait Lens working in the visible spectral range at relative aperture F/3. Table 5 summarizes the data for the CHI Telescope. By applying (17) to the CHI Telescope one finds for the total amount of aberrations:  $\Delta l'_k \approx 2 \cdot b \cdot \Delta I = 2 \cdot 2.48 \cdot 6.4\mu\text{m} \approx 31.8\mu\text{m}$ . The optical CAD does not allow for a comparison neither of the aberration nor of the NA.

Table 5 Helmholtz-Lagrange Invariant of the nominal design of the CHI freeform Telescope [7].

<i>At the entrance Aperture</i>		<i>At the image plane</i>	
Semi-Entrance Pupil [mm]	75,00	Radial Marginal ray angle [°]	-21,0672
Radial FoV (3.24°, 0.22°) [°]	3,2475	NA (0,0,1,0)	0,2014
$n_1 \cdot q_1 \cdot \sin(w_1)$ [mm]	4,2486	$n'_k \cdot \tilde{l}'_k \cdot \sin(u'_k)$ [mm]	-4,2423

Figure 11 reports the total amount of residual aberration  $\Delta l'_k$  for the CHI and the TIR Telescope as a function of the entrance pupil height. The quantity  $\Delta l'_k$  is calculated with the formula (17).

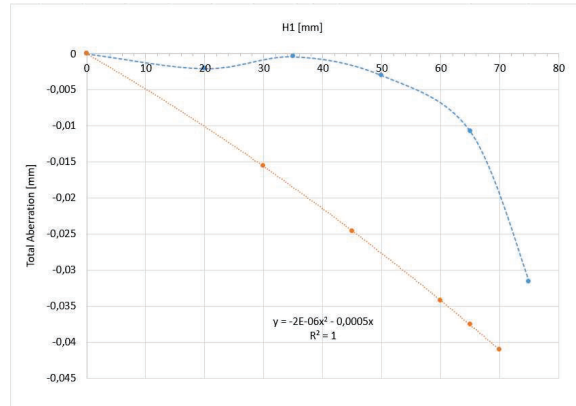


Figure 11  $\Delta l'_k$  as a function of the entrance pupil radial aperture for the CHI (pointed curve) and TIR Telescope (dashed curve).

The polychromatic spot diagram of a Petzval Portrait Lens, used as an example of a pure refractive Lens, is shown in left panel of Figure 12. For this lens it results:  $I = 0.3479$  mm at Entrance Pupil and  $I = -0.3486$  mm at image plane. The change in the  $I$  from object to image plane is approximately  $1.0 \mu\text{m}$  in line with the dimensions of the spot diagrams. By applying (17) to this Petzval Lens one finds:  $\Delta l'_k \approx 2 \cdot \Delta I \cdot b = 2 \cdot 0.7 \mu\text{m} \cdot 3.048 \approx 4.3 \mu\text{m}$  well in line with the data of right panel of Figure 12, where summing spherical aberration and field curvature one obtains approximately  $4.5 \mu\text{m}$ .

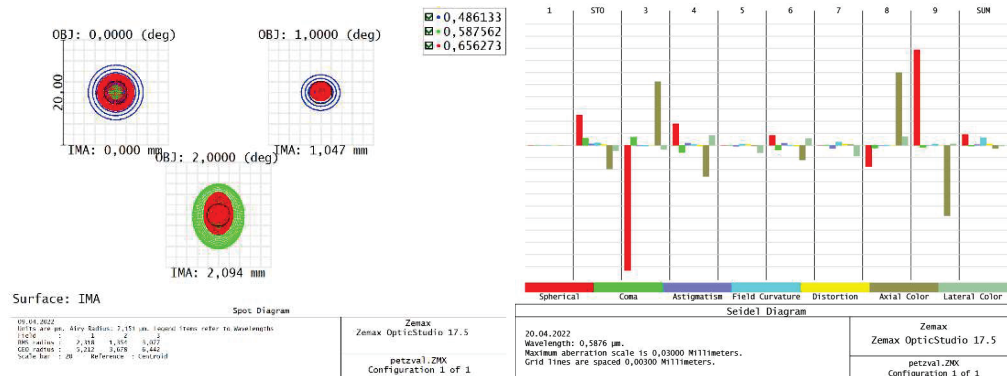


Figure 12 Left /Right: Polychromatic spot / Seidel diagram of a Petzval Portrait Lens with 1:3, used as a cross-check example.

Following Table 6 summarizes the values of the  $I$  at the image plane, the WFE rms and spot rms of the nominal design and of the design subjected to a set of MAIT tolerances. The tolerances are also relaxed a factor 2 and the calculation is repeated.

Table 6 Helmholtz-Lagrange Invariant, WFE rms, spot rms of a Petzval Lens with 1:3. Nominal design and with MAIT tolerances.

	MAIT tolerances			2x loosened MAIT tolerances		
	$ I $ [mm] at image plane	WFE rms FoV max [waves]	rms Spot FoV max [mm]	$LLW$ [mm] image plane	WFE rms FoV max [waves]	rms Spot FoV max [mm]
Nominal	0,3486	0,19904	0,0031	0,3486	0,1990	0,0031
Max.	0,3546	0,2828	0,0044	0,3590	0,4363	0,0063
Min.	0,3438	0,1040	0,0022	0,3395	0,0688	0,0016
Average	0,3487	0,2107	0,0032	0,3488	0,2330	0,0035
St. Dev.	0,0020	0,0304	0,0003	0,0040	0,0624	0,0007

We find that the standard deviation of the Helmholtz-Lagrange invariant is almost coincident with the rms spot radius. Interesting to note that  $I$ ,  $WFE_{rms}$  and  $spot_{rms}$  change with the same ratio as the relaxing factor of the set of tolerance.

### 9. DEPTH OF FOCUS FROM HELMHOLTZ-LAGRANGE INVARIANT

As a last exercise we note, how the above defined system invariant expressed with the (8) and its equivalent form (9), allows for the evaluation of the depth of focus, re-obtaining the well-known Kingslake's Formula [17], [18] and [19] of the every-day life of an optical engineer. In this Section we use in great part the theory presented in [12].

Let's assume to shift the image plane along the optical axis, due for example to MAIT tolerances, and let's evaluate the amount of shift that can be tolerated by the system under interest. With reference to right panel of Figure 13 a shift of the image plane from  $O'$  to  $O'^*$  introduces a blurring  $A'^* = \Delta l'_k$  of the image. With the symbol  $*$  we indicate the shifted plane and the related quantities. The distance  $\xi$  corresponding to the blurred image  $A'^*$  can be evaluated by means of eq. (16). In fact by comparing the value of the change in the system invariant with the Rayleigh quarter-wave criterion, one obtains the value of the distance  $\xi$  for which the change in the quantity  $I$ , due to the blurring of the image, can be tolerated by the system. In formulas this means:

$$\Delta I \approx A'^* n' \sin(u') = \pm \frac{\lambda}{4} \quad (18).$$

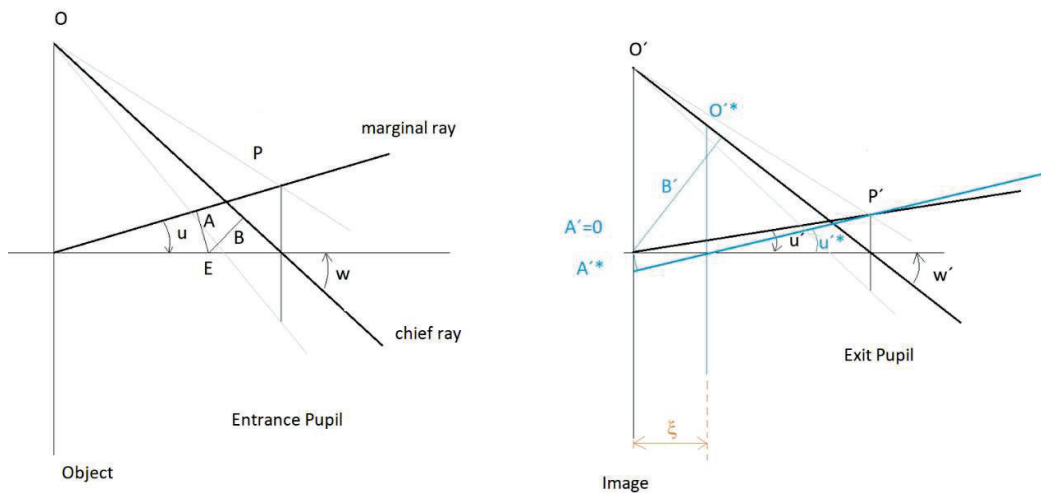


Figure 13 Left / Right panel: object space  $O$  and image space  $O'^*$  [12].

For the distance  $\xi$  one obtains simply from the trigonometry:

$$\xi = \frac{A'^*}{n'^* \sin(u'^*)} \quad (19)$$

Combining (17) and (18) one obtains for the distance  $\xi$ :

$$\xi = \frac{A'^*}{n'^* \sin(u'^*)} \approx \pm \frac{\lambda}{4} \cdot \frac{1}{n'^* \sin(u'^*) \cdot n' \sin(u')} \approx \pm \lambda \cdot b^2 \quad (20)$$

being  $n'^* U'^* \approx n' U'$  the image space numerical aperture,  $b$  the relative Aperture and  $f$  the focal length of the objective, linked by the relation  $NA = \frac{1}{2b}$ . Formula (20) represents the well-known Kingslake formula for the depth of focus, e.g. [18] and [19], when the object is at infinity.

## 10. CONCLUSIONS

The paper presents the TIR freeform Telescope designed by OHB Germany with its main optical properties and with the foreseen optical characterization campaign. The preparation of the set-ups for the optical measurements gave us the opportunity to use the geometric optic for a deeper understanding of the main properties of the telescope. In particular, the use of the Helmholtz-Lagrange invariant worked out to be a useful tool for roughly estimating the residual aberrations of an optical design and also for assessing its robustness wrt to a selected set of MAIT tolerances, de-correlated from the commonly used image quality parameters. This approach results useful in those cases, e.g. telescopes with freeform optics, when the optical CAD does not evaluate first order parameters and Seidel aberrations. Formulas (16) and (17) have been tested with optical systems working as fast as 1:2.4 and also with slower ones obtaining good agreement with the results from optical CAD.

## REFERENCES

- [1] J. Reimers, A. Bauer, K. P. Thompson, and J. P. Rolland, *Freeform spectrometer enabling increased compactness*, Light Sci. Appl. 6, e17026 (2017).
- [2] A. Bauer, E. M. Schiesser, and J. P. Rolland, *Starting geometry creation and design method for freeform optics*, Nat. Commun. 9, 1–11 (2018).
- [3] W. Hou, J. Zhu, T. Yang, and G. Jin, *Construction method through forward and reverse ray tracing for a design of ultra-wide linear field-of-view off-axis freeform imaging systems*, J. Opt. 17, 055603.
- [4] M. P. Chrisp, *Wide angle reflective telescopes with NURBS freeform surfaces*, Proc. SPIE 10590, 1059011 (2017).
- [5] M.D. Nijkerk et al. *Freeform optics design tool for compact spectrometers*. Proc. of SPIE Vol. 11180 1118022-1. ICSO 2018.
- [6] M. Beier et al. *Development, fabrication, and testing of an anamorphic imaging snap-together freeform telescope*, Appl. Opt. 54, 3530–3542 (2015).
- [7] M. Deiml et. al. *Development of a Freeform Telescope for a Compact and Highly Performant Hyperspectral Imager*, 4S Symposium (2022).
- [8] J. P. Rolland et al. *Freeform optics for imaging*, Optica Vol. 8, No. 2 / February 2021 / p. 161.
- [9] G. W. Forbes, *Characterizing the shape of freeform optics*, Opt. Express 20, 2483–2499 (2012).
- [10] N. Takaki et al. *On-the-fly surface manufacturability constraints for freeform optical design enabled by orthogonal polynomials*, Opt. Express 27, 6129–6146 (2019).
- [11] <https://support.zemax.com/hc/en-us/articles/1500005576322-Freeform-optics-in-OpticStudio>
- [12] H. G. Zimmer, *Geometrische Optik*, Springer Verlag (1967), K. 15, S. 42.
- [13] M. Berek, *Grundlagen der praktischen Optik*, Walter de Gruyter & Co. (1970), K. 2, S. 17.
- [14] M. Born and E. Wolf, *Principles of Optics* (Pergamon, 1980), Chap. 4.4.5, P. 165.
- [15] Zemax Optic Studio and Zemax Optic Studio User Manual.
- [16] E. Delano, *First order Design of the  $y, \bar{y}$ , Diagram*, Appl. Opt. 2, 1251-1256 (1963).
- [17] H. Gross, *Design and Correction of Optical Systems*, www.iap.uni-jena.de (2014).
- [18] M. Laikin, *Lens Design*, CRC Press.
- [19] W. J. Smith, *Modern Optical Engineering*, SPIE, Press, McGraw-Hill, 3rd Ed. (2000).